INFLUENCE OF WALL TEMPERATURE ON THERMAL EFFECT OF NOZZLE FLOWMETER

Yu-Liang Zhang[a], Liang-Huai Tong[b], Jun-Jian Xiao[a,†], Kai-Yuan Zhang[c]

[a] *College of Mechanical Engineering & Key Laboratory of Air-driven Equipment Technology of Zhejiang Province, Quzhou University, Quzhou, Zhejiang, 324000, China*
[b] *Quzhou Special Equipment Inspection Center, Quzhou, Zhejiang, 324000, China*
[c] *School of Mechanical Engineering, Hunan University of Technology, Zhuzhou, Hunan, 412007, China*

ABSTRACT

Nozzle flowmeter has simple structure and wide application. In order to study the influence of temperature change on the inner wall of nozzle flowmeter on the thermal effect of flowmeter, the thermal effect of nozzle flowmeter was numerically simulated at five different inner wall temperatures in this paper. It is found that with the increase of the inner wall temperature, obvious stress concentration occurs in the upstream and downstream pressure inlets and the inlet and outlet areas of the flowmeter, and the thermal stress increases with the increase of the wall temperature. There are large thermal deformation areas in the inlet and outlet areas of the upstream and downstream pressure inlets and the eight-slot nozzle, and the thermal deformation value increases with the increase of wall temperature.

Keywords: *Nozzle, Flowmeter, Thermal effect, Wall temperature, Numerical simulation*

1. INTRODUCTION

Steam metering is widely used in industrial production. Steam flow meters are mostly installed in high temperature and high-pressure steam pipelines, which are not convenient for disassembly. How to improve the field detection technology of steam flow meters becomes very important. Many scholars have studied the internal flow and external characteristics of various types of flowmeters from different perspectives. Shah *et al.* (2012) analyzed the distribution characteristics of velocity field and pressure field downstream the orifice plate in detail through numerical simulation, the variation laws of turbulent kinetic energy and turbulent dissipation rate in different regions, and the relationship between flow rate and pressure drop. Liu *et al.*(2015) numerically simulated the internal flow of V-cone flowmeter, and found that there was a large-scale vortex ring downstream of the cone. According to the flow analysis of outlet wake field, the single support structure of V-cone was changed to double support structure, which improved the repeatability of flow coefficient. Lavante *et al.*(2000) found that there was obvious unstable flow and large-scale flow separation in the critical flow Venturi tube through simulation, resulting in the decrease of measured flow and the fluctuation of flow coefficient. Cui *et al.* (2015, 2014) simulated the internal flow distribution of the precession vortex flowmeter. The pressure loss performance of the flowmeter could be improved by increasing the guide distance of the cyclone blade and the throat diameter of the flowmeter at the same time. Zhang *et al.* (2005) adopted CFD numerical simulation method to effectively reduce pressure loss by changing the number of spiral blades and blade incidence angle of the swirler of precession vortex flowmeter.

Irving *et al.* (1979) carried out an experimental study on the measurement performance of orifice flowmeter under turbulent flow, analyzed the influence of different installation conditions on measurement, and obtained the quantitative change of flow coefficient

under turbulent flow. Singh *et al.* (2009, 2010) found that the increase of the vortex angle of the upstream vortex flow affected the pressure distribution in the flowmeter and the flow field structure downstream of the cone, which led to the increase of the flow coefficient of the flowmeter through numerical simulation. In 1994, Hakansson *et al.* (1994) found that the measurement error of ultrasonic flowmeter was directly proportional to the pulsation amplitude and inversely proportional to the pulsation frequency by analyzing the effects of pulsation amplitude, pulsation frequency and average flow velocity. In addition, Venugopal *et al.* (2012) studied the effect of valve and vortex flow on vortex shedding frequency of vortex flowmeter, and analyzed the influence of vortex structure on measurement under disturbed flow. Manshoor *et al.* (2011) found that different forms of upstream turbulence would affect the internal flow and cause measurement error through comparative analysis of numerical simulation. The numerical simulation method is also used to reveal other internal characteristics (Abed *et al.*, 2020; Gu *et al.*, 2020).

Nozzle flowmeter effectively solves the problem of traditional orifice plate in measurement and is being more and more widely used. When the fluid flows through the nozzle, it is not like the orifice plate that suddenly changes the flow state of the fluid. A nozzle with a smaller opening diameter than the inner diameter of the pipeline is placed in the pipeline. When the pipeline is filled with fluid and the fluid flows through the nozzle, the flow velocity will cause local contraction near the nozzle plate, and the static pressure difference between the upstream and downstream of the nozzle is generated. The static pressure difference can be used to monitor the flow of the fluid in real-time online. In addition, the nozzle has a small resistance drop and a large differential pressure, and the use of nozzle flowmeters makes fluid flow more stable, which makes nozzle is increasingly popular as a substitute for orifice plate in oil field applications. The structural performance of the nozzle is largely affected by the internal structure and flow field distribution. As a differential pressure flowmeter, nozzle

---

steam flowmeter is widely used in flow measurement of high temperature and high-pressure fluids in power and chemical industries.

However, the current research on flowmeters mainly focuses on the accuracy calibration of steam flowmeters, and the analysis of flowmeter thermodynamics is less. In this paper, the influence of different inner wall temperature on the thermal effect of nozzle flowmeter is studied based on numerical simulation method.

2. PHYSICAL MODEL AND COMPUTATIONAL METHOD

The nozzle flowmeter is mainly composed of front measuring tube, rear measuring tube, nozzle and weld metal. The specific structure and sectional view of flow meter are shown in Fig. 1.
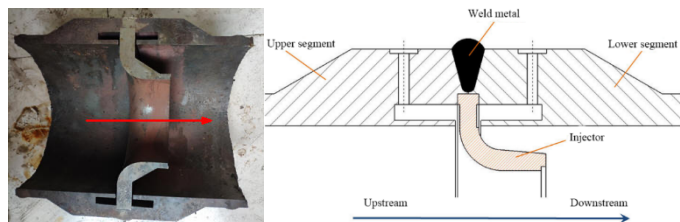

Fig. 1 Overall structure diagram

2.1 Measurement Tube

Because the nozzle flowmeter is axisymmetric model, the parameters of the front measurement tube and the rear measurement tube are the same. Figure 2 shows the size of the measuring tube before the nozzle flowmeter, in which the inlet diameter of the measuring tube is 213 mm, the overall diameter of the measuring tube is 358 mm, and the outlet diameter of the measuring tube is 223 mm. A number of upstream and downstream pressure outlets with a diameter of 27 mm are distributed around the measuring tube. The material of the measuring tube is 12CrMoVG.
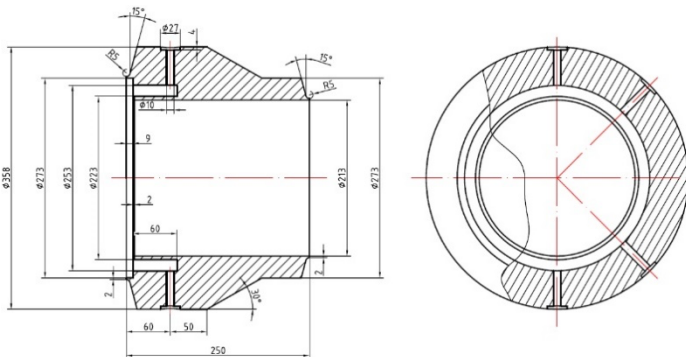

Fig. 2 Measurement tube size diagram

2.2 Eight-slot Nozzle

Figure 3 shows the size of the eight-slot nozzle of the nozzle flowmeter. The inlet diameter of the eight-slot nozzle is 213 mm, the overall diameter of the eight-slot nozzle is 273 mm, and the outlet diameter of the eight-slot nozzle is 127.8 mm. A number of grooves with a depth of 2 mm are distributed around the measuring tube. The material of eight-slot nozzle is 304 stainless steel, 06Cr19Ni10 stainless steel is a common material.
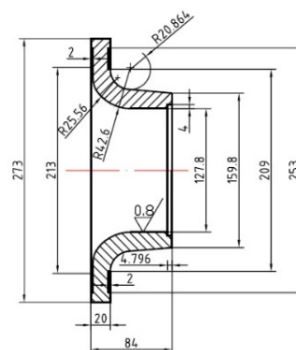

Fig. 3 Dimensions of eight-slot nozzle

The weld metal is mainly used for measuring tube and eight-groove nozzle before and after connection. The weld radius of the weld metal is 5 mm and the weld deflection angle is 30°.

2.3 Governing Equation

The heat conduction equation is as following in this paper.

$$q = -\lambda \, grad \, t = -\lambda \frac{\partial t}{\partial n} n \tag{1}$$

2.4 3D Model and Meshing

The three-dimensional modeling software UG was used to conduct the proportional three-dimensional modeling of the solid structure of the nozzle flowmeter, and the solid models of the solid structures such as the front measuring tube, the rear measuring tube, the eight-groove nozzle and the weld metal were obtained. Figure 4(a) shows the calculation domain of solid structure of the nozzle flowmeter. In this paper, ICEM software is used to grid the solid structure domain of nozzle flowmeter. Unstructured tetrahedron mesh with better adaptability is used for complex computational domains such as front measuring tube, rear measuring tube, eight-slot nozzle and weld metal. The grid number dependence test is also carried out with several grid numbers. Results show when the relative error of the observed head is less than 2%, the effect of grid number can be ignored. The final total number of grids is 100,000, and the grid diagram of solid structure is shown in Fig. 4(b).
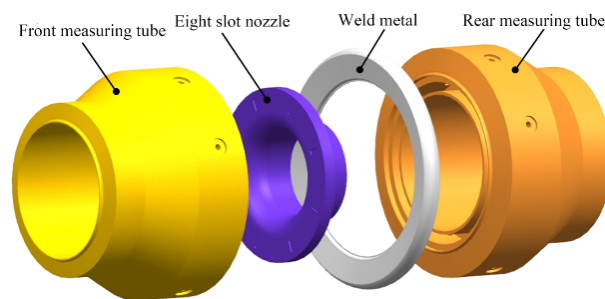
(a) Solid structure
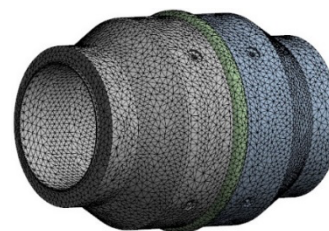
(b) Grid diagram

Fig. 4 Solid structure and grid diagram

3. CALCULATION SCHEME

All calculation boundary are solid wall. The specific settings of boundary condition in this paper are as follows:

(1) The temperature at outer wall of the flowmeter is set as 20℃, and the temperature at inner wall is set as 50℃, 100℃, 300℃, 500℃ and 700℃ respectively.

(2) The material of the measuring tube is set as 12CrMoVG, and the specific material properties are as follows: Tensile strength σ_b (MPa): ≥490(50); Yield strength σ_s (MPa): ≥245(25); Elongation δ (%): ≥22. Section shrinkage ψ (%): ≥50. Impact energy Akv (J): ≥71. Impact toughness value αkv (J/cm^2): ≥88(9). Hardness: ≤179HB.

(3) The material of the measurement tube is 304 stainless steel 06Cr19Ni10, and the specific material properties are as follows: Density ρ=7.93 g/cm^3, tensile strength σ_b (MPa) ≥ 515-1035. The conditional yield strength σ (MPa) ≥ 205. Elongation δ_5 (%) ≥ 40. Specific heat capacity (0~100℃, KJ·kg^{-1}K^{-1}): 0.50. Thermal conductivity (W·m^{-1}·K^{-1}): (100℃) 16.3, (500℃) 21.5. Longitudinal elastic modulus (20℃, KN/mm^2): 193.

(4) The material of weld metal is set as H08CrMoVA, and the specific material properties are as follows: Tensile strength σ_b/MPa): ≥ 1180, yield point (σ_s/MPa): ≥ 885, elongation after fracture (δ/%): ≥ 10, section shrinkage (ψ/%): ≥ 45, impact absorption energy (Aku2/J): ≥ 55, and Brinell hardness (annealing or high temperature tempering): ≤ 21.

4. RESULT ANALYSIS

In this paper, ANSYS software is used to calculate the thermal effect of nozzle flowmeter under different inner wall temperature. The steady-state thermal effect of the solid structure of the nozzle flowmeter was numerically calculated at the inner wall temperature of 50℃, 100℃, 300℃, 500℃ and 700℃, and the temperature field, thermal stress and thermal deformation distribution of the cross section of the nozzle flowmeter at different inner wall temperatures were compared and analyzed.

4.1 Temperature Field Analysis

Figure 5 shows the cross-sectional temperature field distribution diagram of the nozzle flowmeter under different inner wall surface temperatures. When the temperature of the outer wall surface remains unchanged at 20℃, the internal temperature field distribution of the nozzle flowmeter gradually generates heat transfer as the temperature of the inner wall surface increases. When the temperature of the inner wall surface rises from 50℃ to 700℃, the internal temperature field of the flowmeter shows obvious stratification as the temperature rises. When the temperature of the inner wall surface of the nozzle flowmeter is 700℃, most of the inside of the nozzle flowmeter is in a high temperature state, and the area of the low temperature area on the outer wall surface is small. At the same time, the temperature distribution in the upstream and downstream pressure test space is also more obvious. When the temperature of the inner wall of the nozzle flowmeter is 50℃, the internal temperature distribution is mainly concentrated in the low temperature section, and the heat transfer is weak.

Figure 6 shows a schematic diagram of the detection path of the upstream and downstream pressure taps of the nozzle. It can be seen from Fig. 6(c) that the monitoring path 1 is a path from the upstream pressure taking port A1 point parallel to the gas flow direction to the downstream pressure taking port A2. The monitoring path 2 is a path from the inner wall surface B1, which is perpendicular to the gas flow direction, to the outer wall surface B2. The paths 1 and 2 are monitored respectively, and the influence of different inner wall surface temperatures on the temperature field and heat flow field distribution on paths 1 and 2 is obtained.
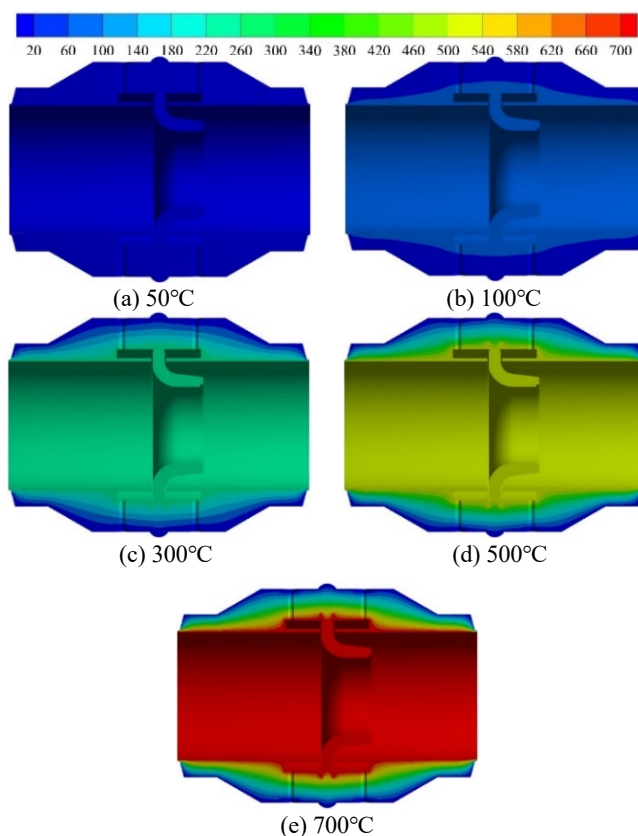

(a) 50℃   (b) 100℃

(c) 300℃   (d) 500℃

(e) 700℃

Fig. 5 Temperature field distribution

(a) Monitoring path 1   (b) Monitoring path 2
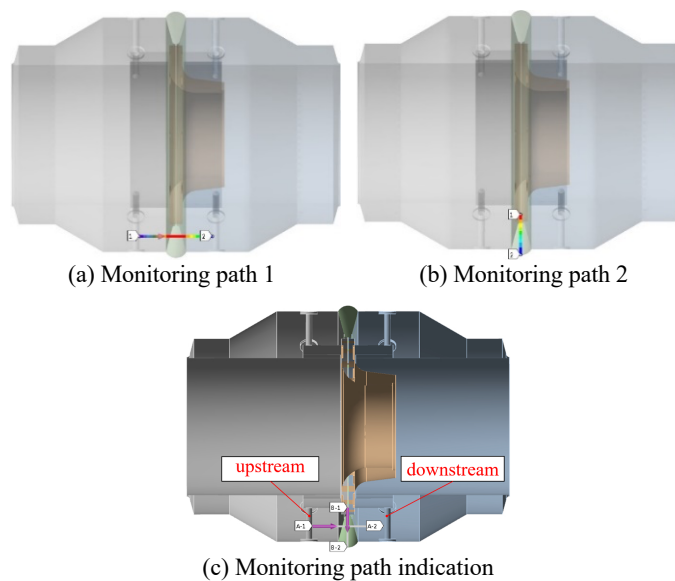
(c) Monitoring path indication

Fig. 6 Schematic diagram of detection path for nozzle upstream and downstream intake

Figure 7 shows the temperature field distribution of the monitoring path 1 under different inner wall surface temperatures. Under different inner wall surface temperatures, the temperature distribution on the path from the upstream pressure port to the downstream pressure port has a trend of first increasing and then decreasing, and they all reach a temperature peak at 0.5L. When the inner wall temperature of the nozzle flowmeter is 50℃, 100℃, 300℃, 500℃ and 700℃, the maximum temperature of the monitoring path 1 are 33.7℃, 56.62℃, 148.17℃, 239.72℃ and 331.27℃ respectively. It can be seen that as the temperature of the inner wall surface of the nozzle flowmeter increases, the temperature peak of the monitoring path 1 also increases.

When the inner wall temperature of the nozzle flowmeter is 50℃, 100℃, 300℃, 500℃ and 700℃, the maximum amplitude (maximum peak value-minimum valley value) of monitoring path 1 is 2.04℃, 5.53℃, 19.34℃ ,33.16℃ and 46.97℃ respectively. It can be seen that as the temperature of the inner wall surface increases, the maximum amplitude of the monitoring path 1 also increases.
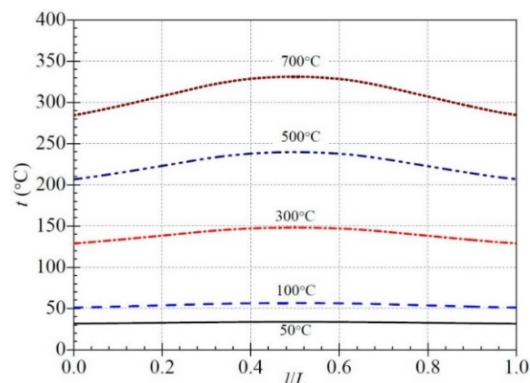

Fig. 7 Temperature distribution of monitoring path 1

Figure 8 shows the temperature field distribution of the monitoring path 2 under different inner wall surface temperatures. It can be seen that at different inner wall surface temperatures, the temperature distribution on the path from the inner wall to the outer wall surface gradually decreases, and both reach the maximum at 0L and the minimum at 1.0L. When the inner wall temperature of the nozzle flowmeter is 50℃, 100℃, 300℃, 500℃ and 700℃, the maximum temperature of monitoring path 2 are 48.573℃, 96.195℃, 286.68℃, 477.17℃ and 667.66℃ respectively. It can be seen that as the temperature of the inner wall surface of the nozzle flowmeter increases, the maximum value of the monitoring path 2 also increases. When the inner wall temperature of the nozzle flowmeter is 50℃, 100℃, 300℃, 500℃ and 700℃, the maximum amplitude (maximum peak value-minimum valley value) of monitoring path 2 is 28.38℃, 75.67℃, 264.87℃ ,454.06℃ and 643.255℃ respectively . It can be seen that as the temperature of the inner wall surface of the nozzle flowmeter increases, the maximum amplitude of the monitoring path 2 also increases.
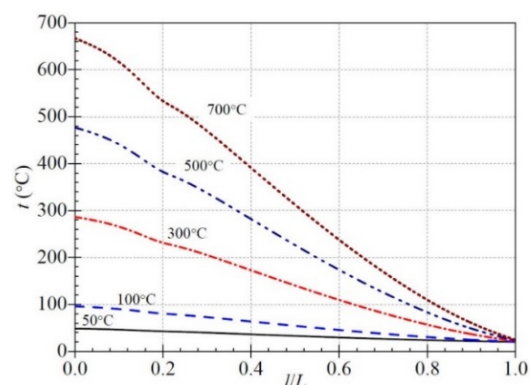

Fig. 8 Temperature distribution of monitoring path 2

4.2 Thermal Stress Analysis

Figure 9 is a graph of the thermal stress distribution in the cross-section of the nozzle flowmeter under different inner wall surface temperatures. It can be seen that when the temperature of the outer wall surface remains unchanged at 20℃, the average thermal stress inside the nozzle flowmeter increases with the increase of the temperature. When the temperature reaches 50℃, the internal thermal stress value of the nozzle flowmeter is lower than 10Pa, and there is no obvious stress

concentration inside the flowmeter. When the temperature of the inner wall surface rises to 100℃, the overall thermal stress value inside the nozzle flowmeter is still low, and a 510Pa low-strength stress concentration phenomenon occurs at the upstream and downstream pressure taps of the flowmeter. When the temperature of the inner wall surface is 300℃, the internal thermal stress value of the nozzle flowmeter has a relatively obvious increase, and the stress concentration phenomenon is mainly concentrated in the internal upstream and downstream pressure taps and the vicinity of the flowmeter inlet and outlet. The maximum stress value is 1010Pa. When the temperature of the inner wall surface is 500℃, there is a more obvious stress concentration phenomenon in the upstream and downstream pressure port area of the flowmeter, and the maximum stress value is 2510Pa. When the temperature of the inner wall surface rises to 700℃, obvious stress concentration occurs at the upstream and downstream pressure inlets and inlet and outlet areas of the flowmeter, and the maximum stress value is 2510Pa.
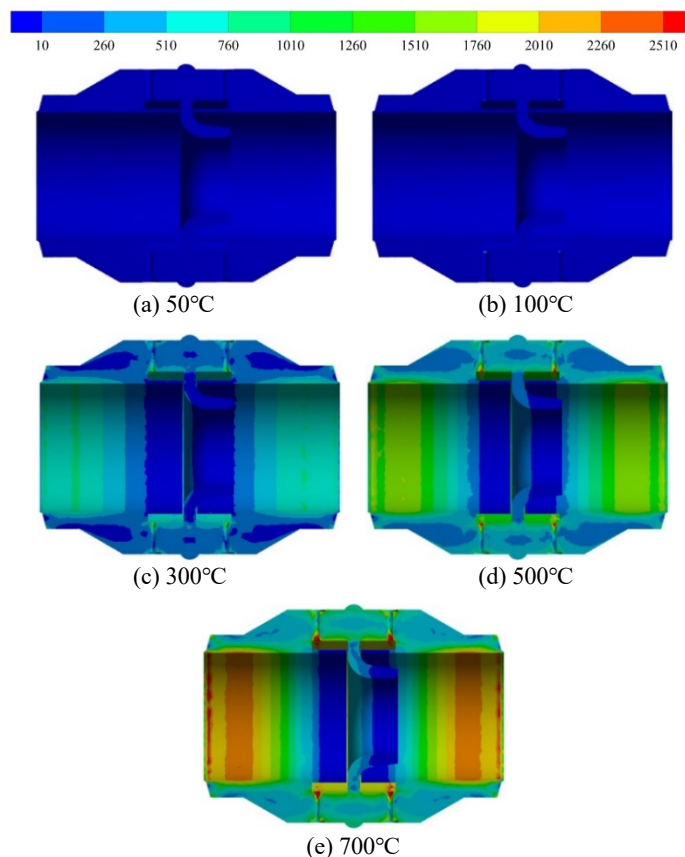

Fig. 9 Thermal stress distribution

Figure 10 shows the thermal stress distribution of the monitoring path 1 under different inner wall surface temperatures. It can be seen that under different inner wall temperatures, the thermal stress distribution on the path from the upstream pressure port to the downstream pressure port has a trend of first decreasing and then increasing, and all reach the valley value at 0.5L. When the inner wall temperature of the nozzle flowmeter is 50℃, 100℃, 300℃, 500℃ and 700℃, the maximum peak value of monitoring path 1 are 42.63Pa, 118.81Pa, 423.61Pa, 728.41Pa and 1033.2Pa respectively. The maximum valley value of monitoring path 1 is 22.25Pa, 64.28Pa, 232.74Pa, 401.23Pa and 569.73Pa respectively. It can be seen that as the temperature of the inner wall surface of the nozzle flowmeter increases, the peak and valley values of the thermal stress of the monitoring path 1 increase accordingly. When the inner wall temperature of the nozzle flowmeter is 50℃, 100℃, 300℃, 500℃ and 700℃, the maximum amplitude (maximum peak value-minimum valley

value) of monitoring path 1 is 20.11Pa, 54.53Pa, 190.87Pa, 327.18Pa and 463.47Pa respectively. It can be seen that as the temperature of the inner wall surface of the nozzle flowmeter increases, the maximum amplitude of the monitoring path 1 also increases.
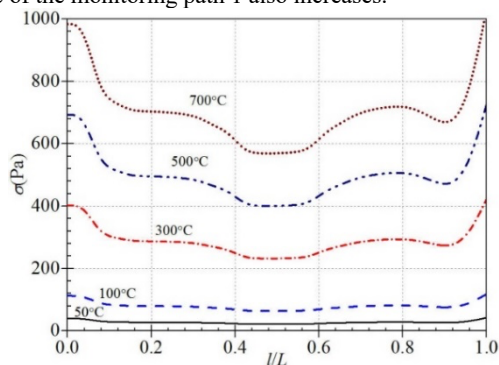

Fig. 10 Thermal stress distribution of monitoring path 1

Figure 11 shows the thermal stress distribution of the monitoring path 2 under different inner wall surface temperatures. It can be seen that at different inner wall temperatures, the temperature distribution on the path from the inner wall to the outer wall first increases, then decreases and then increases, and both reach the maximum and minimum at 0.15L and 0.46L respectively. When the inner wall temperature of the nozzle flowmeter is 50°C, 100°C, 300°C, 500°C and 700°C, the maximum values of monitoring path 2 are 51.56Pa, 144.25Pa, 515.08Pa, 885.91Pa and 1256.8Pa respectively. The minimum values of monitoring path 2 are 22.02Pa, 64.07Pa, 232.56Pa, 401.08Pa and 569.6Pa respectively. It can be seen that as the temperature of the inner wall surface of the nozzle flowmeter increases, the maximum and minimum values of the monitoring path 2 also increase. When the inner wall temperature of the nozzle flowmeter is 50°C, 100°C, 300°C, 500°C and 700°C, the maximum amplitude (maximum peak value-minimum valley value) of monitoring path 2 is 29.54Pa, 80.18Pa, 282.52Pa , 484.83Pa and 687.2Pa respectively. It can be seen that as the temperature of the inner wall surface of the nozzle flowmeter increases, the maximum thermal stress amplitude of the monitoring path 2 also increases.
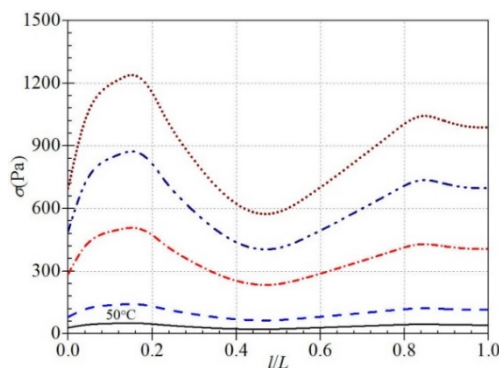

Fig. 11 Thermal stress distribution of monitoring path 2

4.3 Thermal Deformation Analysis

Figure 12 shows the thermal deformation distribution diagram of the cross section of the nozzle flowmeter under different inner wall surface temperatures. It can be seen that when the temperature of the outer wall surface remains unchanged at 20°C, the average thermal deformation value inside the nozzle flowmeter increases with the increase of the temperature of the inner wall surface. When the temperature of the inner wall surface is 50°C and 100°C, the internal thermal deformation value of the nozzle flowmeter is lower than 0.13mm, and there is no obvious stress concentration inside the flowmeter. When the temperature of the inner wall surface is 300°C, the internal thermal deformation value of the nozzle flowmeter has a relatively obvious

increase. The large deformation area is mainly concentrated in the internal upstream and downstream pressure taps and near the inlet and outlet of the eight-slot nozzle. The maximum thermal deformation value is 0.39mm. When the temperature of the inner wall surface is 500°C, there are obvious thermal deformation areas at the upstream and downstream pressure taps of the flowmeter and the outlet of the eight-slot nozzle, and the maximum stress value is 0.78mm. When the temperature of the inner wall surface rises to 700°C, the thermal deformation value of the larger thermal deformation area at the upstream and downstream pressure tapping ports of the flowmeter and the inlet and outlet of the eight-slot nozzle has increased significantly, and the maximum thermal deformation value is 1.3 mm. It can be seen that as the temperature of the inner wall surface of the nozzle flowmeter rises, the maximum thermal deformation amplitude inside it also increases.
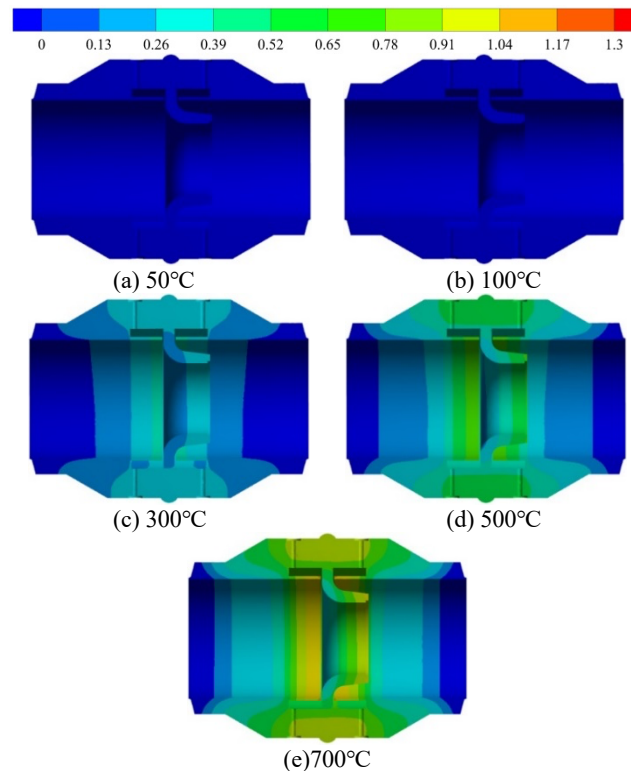

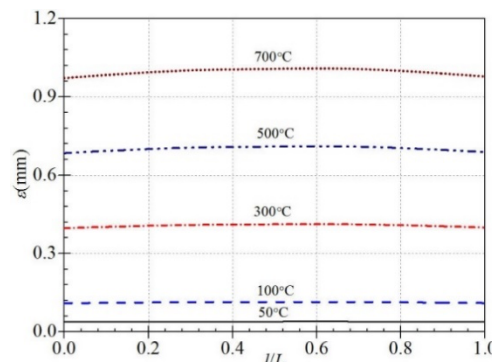**Fig. 12** Thermal deformation distribution

Fig. 13 Thermal deformation distribution of monitoring path 1

Figure 13 shows the thermal deformation distribution of the monitoring path 1 under different inner wall surface temperatures. It can be seen that under different inner wall surface temperatures, along the path from the upstream pressure inlet to the downstream pressure inlet, the thermal deformation distribution showed a trend of first increasing and then decreasing, and both reached a peak at 0.58L. When the inner wall temperature of the nozzle flowmeter is 50°C, 100°C, 300°C, 500°C and 700°C, the maximum peak values of

monitoring path 1 are 0.039mm, 0.11mm, 0.41mm, 0.71mm and 1.01mm respectively. It can be seen that as the temperature of the inner wall surface of the nozzle flowmeter increases, the thermal deformation peak value of the monitoring path 1 also increases.

Figure 14 shows the thermal deformation distribution of the monitoring path 2 under different inner wall surface temperatures. It can be seen that under different inner wall surface temperatures, the thermal deformation distribution on the path from the inner wall to the outer wall surface increases first and then decreases, and both reach the maximum value at 0.65L. When the inner wall temperature of the nozzle flowmeter is 50°C, 100°C, 300°C, 500°C and 700°C, the maximum value of monitoring path 2 is 0.04mm, 0.12mm, 0.42mm, 0.72mm and 1.03mm respectively. It can be seen that as the temperature of the inner wall surface of the nozzle flowmeter increases, the maximum thermal deformation of the monitoring path 2 also increases.
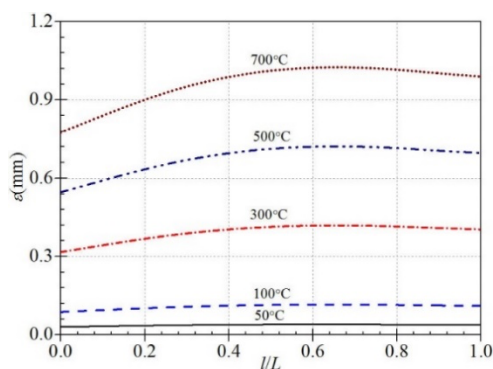

Fig. 14 Thermal deformation distribution of monitoring path 2

5. CONCLUSIONS

With the increase of inner wall temperature, the stress concentration is obvious in the upstream and downstream pressure taps and the inlet and outlet of the flowmeters, and the thermal stress value increases with the increase of wall temperature. With the increase of inner wall temperature, there is a large thermal deformation area in the upstream and downstream pressure taps and the inlet and outlet of the eight-slot nozzle, and the thermal deformation value increases with the increase of wall temperature.

ACKNOWLEDGEMENTS

REFERENCES

Abed, I.M., Ali, H.F., Sahib, S.A.M., 2020, "Investigation of Heat Transfer and Fluid Flow Around Sinsoudal Corrugated Circular Cylinder for Two Dimensional System," *Frontiers in Heat and Mass Transfer*, 15(6), 1–9.
http://dx.doi.org/10.5098/hmt.15.6.

Cui, B.L., Chen, K., Zhu, L.H., Chen, D.S., Huang, D.H., 2014, "Improvement of Structure Design on Swirl Meter Based on CFD," *CIESC Journal*, 65(8), 2963-2969.
https://dx.doi.org/10.3969/j.issn.0438-1157.2014.08.016

Cui, B.L., Lv, Z.Q., Chen, D.S., Chen, K., Huang, D.H., 2015, "Influence of Incident Angle of Swirler on Performance of Swirl Meter," *Transactions of the Chinese Society of Agricultural Engineering (Transactions of the CSAE)*, 31(2), 53-58. (in Chinese with English abstract)
https://dx.doi.org/10.3969/j.issn.1002-6819.2015.02.008

Gu, X.Y., Jiang, G.H., Wo, Y., Chen, B.W., 2020, "Numerical Study on Heattransfer Characteristics of Propylene Glycole-water Mixture in Shell Side of Spiral Wound Heat Exchanger," *Frontiers in Heat and Mass Transfer*, 15(3), 1–8.
http://dx.doi.org/10.5098/hmt.15.3.

Håkansson, E., Delsing, J., 1994, "Effects of Pulsating Flow on an Ultrasonic Gas Flowmeter," *Flow Measurement and Instrumentation*, 5, 93-101.
https://doi.org/10.1016/0955-5986(94)90042-6

Irving, S.J., 1979, "The Effect of Disturbed Flow Conditions on the Discharge Coefficient of Orifice Plates," *International Journal of Heat and Fluid Flow*, 1, 5-11.
https://doi.org/10.1016/0142-727X(79)90019-5

Lavantea, E.V., Zachciala, A., Nath, B., Dietrich, H., 2000, "Numerical and Experimental Investigation of Unsteady Effects in Critical Venturi Nozzles," *Flow Measurement and Instrumentation*, 11, 257-264.
https://doi.org/10.1016/S0955-5986(00)00024-8

Liu, W.G., Xu, Y., Zhang, T., Qi, F.F., 2015, "Experimental Optimization for Dual Support Structures Cone Flow Meters Based on Cone Wake Flow Field Characteristics," *Sensors and Actuators A: Physical*, 232, 115-131.
https://doi.org/10.1016/j.sna.2015.05.019

Manshoor, B., Nicolleau, F.C.G.A., Beck, S.B.M., 2011, "The Fractal Flow Conditioner for Orifice Plate Flow Meters," *Flow Measurement and Instrumentation*, 22(3), 208-214.
https://doi.org/10.1016/j.flowmeasinst.2011.02.003

Shah, M.S., Joshi, J.B., Kalsi, A.S., Prasad, C.S.R., Shukla, D.S., 2012, "Analysis of Flow Through an Orifice Meter: CFD Simulation," *Chemical Engineering Science*, 71, 300-309.
https://doi.org/10.1016/j.ces.2011.11.022

Singh, R.K., Singh, S.N., Seshadri, V., 2010, "CFD Prediction of the Effects of the Upstream Elbow Fittings on the Performance of Cone Flowmeters," *Flow Measurement and Instrumentation*, 21, 88-97.
https://doi.org/10.1016/j.flowmeasinst.2010.01.003

Singh, R.K., Singh, S.N., Seshadri, V., 2009, "Study on the Effect of Vertex Angle and Upstream Swirl on the Performance Characteristics of Cone Flowmeter Using CFD," *Flow Measurement and Instrumentation*, 20(2), 69-74.
https://doi.org/10.1016/j.flowmeasinst.2008.12.003

Venugopal, A., Agrawal, A., Prabhu, S.V., 2012, "Frequency Detection in Vortex Flowmeter for Low Reynolds Number Using Piezoelectric Sensor and Installation Effects," *Sensors and Actuators A: Physical*, 184, 78-85.
https://doi.org/10.1016/j.sna.2012.07.004

Zhang, T., Jia Y.F., Wu, L., 2005, "Research and Improvement of Swirlmeter Based on FLUENT Smiulation," *Control and Instruments in Chemical Industry*, 32(6), 62-64.
https://dx.doi.org/10.3969/j.issn.1000-3932.2005.06.017